












Beyond 110 GHz Uni-Traveling Carrier Photodiodes on an InP-Membrane-on-Silicon Platform

Jasper de Graaf , Xinran Zhao, Dimitrios Konstantinou , Menno van den Hout , *Student Member, IEEE*, Sander Reniers , Longfei Shen, Sjoerd van der Heide , *Student Member, IEEE*, Simon Rommel , *Member, IEEE*, Idelfonso Tafur Monroy , Chigo Okonkwo , *Senior Member, IEEE*, Zizheng Cao , *Member, IEEE*, Ton Koonen , *Fellow, IEEE*, Kevin Williams, *Member, IEEE*, and Yuqing Jiao , *Senior Member, IEEE*

Abstract—In this work we have demonstrated a waveguide integrated uni-traveling carrier photodiode on an InP-membrane-on-silicon platform with 3 dB bandwidth beyond 110 GHz. With design optimization and an improved process, devices as small as $3 \times 2 \mu\text{m}^2$ are successfully realized. An electrical equivalent circuit model based on measured S-parameters revealed ultra-small series resistance and junction capacitance as low as 6.5 Ω and 4.4 fF, respectively, in the diodes. The model also provided insight in the photocurrent dependent characteristics in the bandwidth and responsivity of the devices. Finally, data transmission measurements are demonstrated, showcasing the high speed telecommunication abilities of the UTC-PD.

Index Terms—Photodiode (PD), uni-traveling-carrier photodiode (UTC-PD), nanophotonic, InP-membrane-on-silicon, waveguide integrated.

I. INTRODUCTION

INCREASING demand for high speed data transmission [1] and emerging imaging techniques using frequencies up to the terahertz range [2] generate demand for low-cost and high efficiency millimeter wave to terahertz devices. Approaching these frequency bands using only electronic components has proven to be difficult and requires complex circuits [3]. Photonics based implementations offer a promising alternative by using down-conversion of signals in the optical domain, in combination with a photodetector as photomixer [4]. Using an optically integrated technology to achieve generation of these frequency bands fits the requirements of low cost and high efficiency, providing an interesting alternative to bulky and costly fiber based systems [5].

Manuscript received June 4, 2021; revised August 12, 2021; accepted September 2, 2021. Date of publication September 8, 2021; date of current version September 30, 2021. This work was supported in part by the Institute of Design, Optoelectronics and Sensing (IDEAS) Project INTENSE, Dutch NWO Zwaartekracht Grant “Research Center for Integrated Nanophotonics,” H2020 ICT TWILIGHT Project (contract No. 781471) under the Photonics PPP, and the KPN-TU/e Smart Two Program. (Jasper de Graaf and Xinran Zhao contributed equally to this work.) (Corresponding authors: Jasper de Graaf; Xinran Zhao.)

The authors are with the Institute of Photonic Integration (IPI), Eindhoven University of Technology, 5600 Eindhoven, MB, The Netherlands (e-mail: j.p.d.graaf@tue.nl; xinran.zhao@tue.nl; d.konstantinou@tue.nl; m.v.d.hout@tue.nl; s.f.g.reniers@tue.nl; l.shen@tue.nl; s.p.v.d.heide@tue.nl; simon.rommel@ieee.org; i.tafur.monroy@tue.nl; cokonkwo@tue.nl; z.cao@tue.nl; a.m.j.koonen@tue.nl; k.a.williams@tue.nl; y.jiao@tue.nl).

Color versions of one or more figures in this article are available at <https://doi.org/10.1109/JSTQE.2021.3110411>.

Digital Object Identifier 10.1109/JSTQE.2021.3110411

In particular silicon integrated photonic platforms are of interest due to the ability of integration with CMOS electronic circuits. Germanium based PIN photodiodes on silicon have recently demonstrated bandwidths reaching beyond 110 GHz in combination with bandwidth efficiency products of at least 59.3 GHz [6]. Another promising implementation is based around InP based uni-traveling carrier photodiodes (UTC-PD). These show great performance by demonstrating high responsivity and bandwidth simultaneously [7], resulting in bandwidth efficiency products beyond 55 GHz [8], [9]. The UTC-PD enables high bandwidth operation by only allowing fast electrons to move through the device. Next to this, the absence of holes in the depletion region also reduces the space charge effect, enabling high current operation [10]. Therefore these characteristics make UTC-PDs an interesting device for high speed communications, but also enable the generation of high frequency signals due to its ability to reach bandwidths >100 GHz. Broadband photomixers based around a UTC-PD have already demonstrated reaching frequencies up to 1 THz [11]. The InP based UTC-PD heterogeneously integrated on silicon, reported on in 2016 by Shen [12] demonstrated high bandwidth efficiency products making this approach an interesting alternative to Ge-based PIN PDs on silicon. More recently, the same device demonstrated a bandwidth efficiency product of 55 GHz [13]. The device is realized within the nanophotonic InP-membrane-on-silicon (IMOS) platform which has demonstrated high-density integration of electrically pumped lasers, photodiodes, beam steering devices [14] and a large variety of passive devices, resulting in a high functionality photonic platform [15]. Double-sided processing can be utilized during fabrication enabling an extra degree of freedom in the design of the UTC-PD [12]. The IMOS platform is a promising approach towards the integration of a full-functionality nanophotonic platform on top of Si-based electronic ICs [16].

In this work, an improved design based around the UTC-PD from [12] is realized and analysed, achieving 3 dB bandwidths beyond 110 GHz thanks to reduced diode areas enabled by the use of electron beam lithography. Calibrated responsivity measurements together with simulation results [12] indicate an internal responsivity approximately equal to 0.6 A/W, measured at maximal input power, whereas the optimal bandwidth point of operation is measured at minimal input power. The improved UTC-PD already demonstrated high speed data conversion as

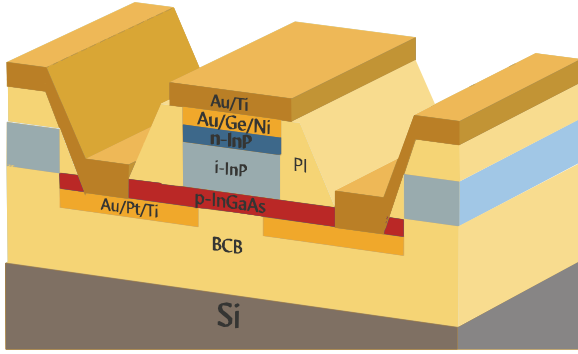


Fig. 1. Simplified schematic representation of the UTC-PD. Sizes not to scale.

key element of an indoor optical wireless link, at a total system transmission of 200 Gb/s [17], [18].

The improved UTC-PD design is characterized as function of device area, at various bias voltages and optical input powers. Equivalent circuit parameters are determined at each point of operation for various PD areas, providing support for the input power and bias voltage dependent characteristics of the devices. This work also demonstrates the high speed data transmission capabilities of the new UTC-PD design by means of eye diagrams and bit error rate (BER) measurements.

II. UTC-PD DESIGN & FABRICATION

Improvements in both design and fabrication are utilized to further increase the bandwidth of the IMOS UTC-PD while maintaining a reasonable responsivity, aiming for a high bandwidth-efficiency product for this InP based PD.

A. UTC-PD Design

The bandwidth of a PD is determined by both the RC bandwidth (f_{RC}) and the carrier transit time bandwidth (f_{tr}) as follows,

$$f_{3\text{ dB}} = \sqrt{\frac{1}{\frac{1}{f_{RC}^2} + \frac{1}{f_{tr}^2}}}. \quad (1)$$

Fig. 1 shows the cross-section of this design, which is in consistency with [12]. The p-type InGaAs (p-InGaAs) layer is used as both the absorption layer and the p-contact layer, the thickness of which is chosen to be 150 nm as an optimization between the absorption efficiency and the diffusion time of electrons through the absorption layer. The doping follows a linear profile ranging from 1×10^{18} to $8 \times 10^{18} \text{ cm}^{-3}$ to induce a quasi field, causing the electrons to drift. The 300 nm intrinsic InP (i-InP) layer is the depletion layer where the electrons drift through, which has the same thickness as the passive waveguide layer on the IMOS platform. The transit time bandwidths are calculated to be 123 GHz and 85 GHz, for the electron overshoot and saturation velocity respectively [12]. f_{RC} is given by

$$f_{RC} = \frac{1}{2\pi\tau_{RC}} = \frac{1}{2\pi RC}, \quad (2)$$

where R is the total resistance and C is the total capacitance. R consists of the series resistance (R_s) and the load resistance. C includes the junction capacitance (C_j) and parasitic capacitances. In Fig. 1, the two Au/Pt/Ti p-contact pads are formed below the p-InGaAs layer using the double-sided processing of the IMOS platform, which leads to a low resistance at the p-side [12]. Meanwhile, the spacing between the two p-contacts is a new degree of freedom in the design. On one hand, putting the p-contacts closer will reduce the series resistance since the distance from the center of the mesa where most holes are generated to the p-contact is reduced. On the other hand, it will increase the optical loss, as the waveguide mode will have increased overlap with the metal contacts. To reduce the series resistance without increasing the optical loss, an additional PD design with a mesa width of $2 \mu\text{m}$ instead of $3 \mu\text{m}$ as used in [12], is included in the fabrication. A narrower mesa also reduces the junction capacitance for a PD of the same length, which enhances the RC bandwidth. f_{RC} can be further boosted by using shorter devices, at an expense of reduced responsivity.

Based on the relation of the PD size to the series resistance and junction capacitance, it was decided to design UTC-PDs in five different lengths ranging from 3 to 30 μm and at widths of 2, 3, & 5 μm resulting in areas from 6 to 150 μm^2 . The UTC-PD sizes in this work are indicated as length \times width. The separation of the p-contacts is set to the width of the respective PD. The estimated 3 dB bandwidths for a $5 \times 2 \mu\text{m}^2$ device are 118 GHz and 83 GHz for the electron overshoot and saturation velocity respectively, while the values for the $10 \times 3 \mu\text{m}^2$ device in [12] are 94 GHz and 73 GHz. The miniaturization of the device requires a more precise patterning technique, which will be discussed in the following section.

B. IMOS UTC-PD Fabrication

The fabrication flow of the UTC-PD follows the process given in [12], which is illustrated in Fig. 2. The devices on the IMOS platform are fabricated using double-sided processing. For the UTC-PD, patterns of the p-side are completed first, as shown in Fig. 2(c). Then, a $2 \mu\text{m}$ thick BCB layer is used to bond the InP sample onto a Si wafer [19]. After bonding, the sample is flipped as shown in Fig. 2(e). With the removal of the InP substrate, processing on the n-side can be performed to complete the formation of the UTC-PDs and other passive devices such as waveguides and grating couplers. One example of the fabricated UTC-PD with the input grating coupler is given in Fig. 2(a).

To achieve the realization of smaller devices, the patterns of p-contacts, p-contact openings and electrodes are formed with e-beam lithography instead of optical lithography as used in [12]. Especially for the p-contact openings and the electrodes, which are formed after bonding when the resolution of the optical lithography is further degraded since the vacuum contact can no longer be ensured due to the uneven sample surface after bonding, the accuracy of patterning can be improved greatly using e-beam lithography. The higher accuracy enables the fabrication of UTC-PD with much smaller sizes than demonstrated in [12], which indeed leads to improvements in device performance as will be shown in the following section.

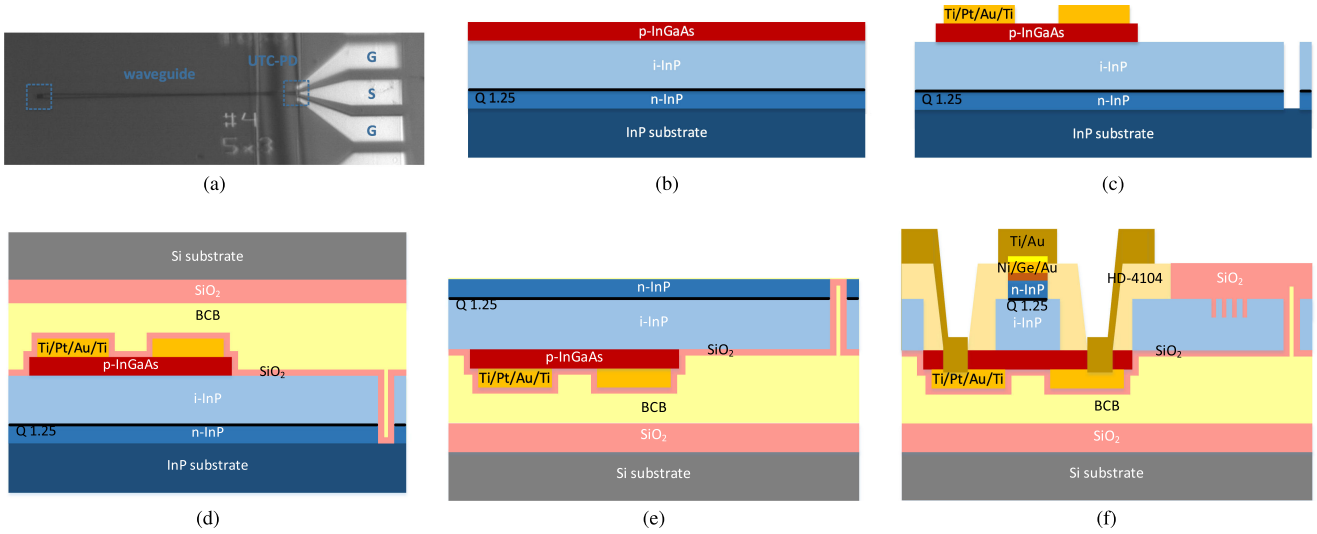


Fig. 2. Fabrication flow of the UTC-PD. (a) SEM image of one fabricated UTC-PD with grating coupler input and ground-signal-ground (GSG) pad output; (b) the initial layer stack of the InP wafer; (c) p-side definition of p-contacts, p-InGaAs, and the alignment markers; (d) the InP wafer is bonded to the Si wafer through a BCB layer; (e) total layerstack after InP substrate removal; (f) n-side definition of n-contacts, waveguides and mesas, grating couplers and electrodes. The p-contact and p-InGaAs are opened to be connected to the ground pad. Polyimide HD-4101 is used for isolation and planarization.

III. CHARACTERIZATION AND ANALYSIS

Apart from the different UTC-PD size variations, both optical and electrical calibration structures are included in the characterization circuits to determine optical losses from the grating couplers and waveguides, as well as the electrical characteristics of the GSG pads. First, basic PD characteristics such as the dark current, photocurrent and responsivity and 3 dB bandwidth are provided. Additionally, the electrical equivalent circuit of the UTC-PD is introduced based on S-parameter measurements, as this enables analysis of the series resistance and junction capacitance of the device, providing detailed insight in the obtained bandwidth results. Finally, data transmission measurements demonstrate the performance of the device in high speed telecommunications.

A. Dark Current and Responsivity Measurements

The setup for the dark current and responsivity measurements is shown in Fig. 3, excluding the VNA and using an external laser at 1550 nm instead. The dark current as function of bias voltages of a $5 \times 2 \mu\text{m}^2$ UTC-PD is plotted in Fig. 4. As explained in [12], the exponential shaped curve suggests that the tunneling current is dominant in this device. The dark current is one magnitude higher than the value in [12], which is caused by a fabrication imperfection. During fabrication, the polyimide planarization layer should be etched back to a height such that the 100 nm thick Au/Ge/Ni n-contact layer was exposed while the n-InP layer underneath was still covered, which was controlled manually with an error margin of 100 nm. If the polyimide was over-etched resulting in the n-InP layer to be exposed, the Ti/Au layer in the final step for the formation of GSG pad would be in contact with the sidewall of the n-InP layer, leading to an increase in the dark current.

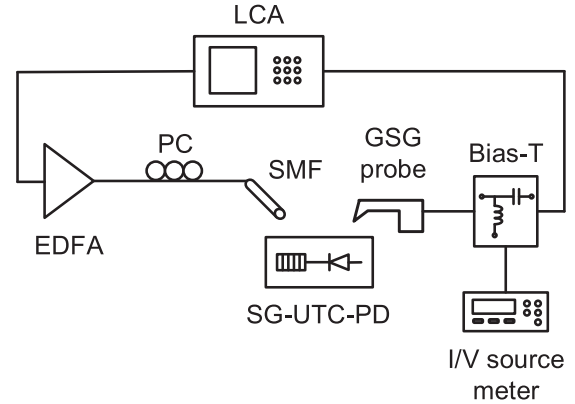


Fig. 3. Schematic measurement setup. EDFA: erbium doped fiber amplifier; PC: polarization controller; SMF: single mode fiber; SG-UTC-PD: surface grating to UTC-PD; GSG: ground-signal-ground; LCA: lightwave component analyzer.

The responsivity of the devices is determined by measuring the photocurrent as function of optical input power, as shown in Fig. 5 for a PD of size $5 \times 2 \mu\text{m}^2$. It can be observed that the results maintain good linearity under low bias and start to show an increasing slope for increased optical input powers when the reverse bias is increased to 2 V and beyond. This is due to a red-shift of the InGaAs bandgap caused by ohmic heating of the absorber [20] that is related to the high dark current of the device [21]. As the responsivity of the device is inversely dependent on the wavelength, as demonstrated in [12], a red-shift of the InGaAs bandgap causes the responsivity to increase, as indicated by the increased slope of the curves at increased optical input powers. The figure also shows the responsivity to be largely dependent on the applied bias, due to the band discontinuity at the InGaAs/InP interface. The necessity of high reverse bias can

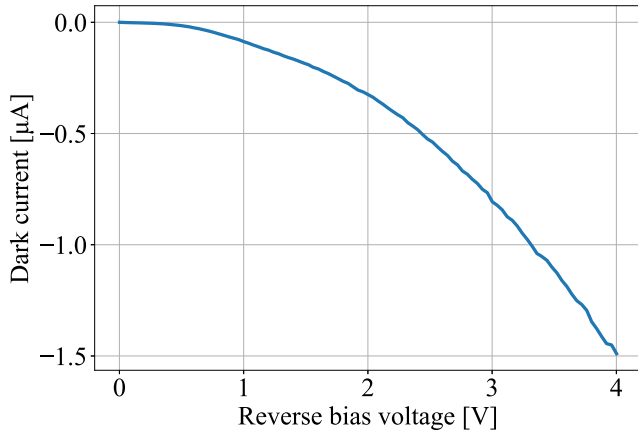


Fig. 4. Dark current as function of bias voltage measured for a $2 \times 3 \mu\text{m}^2$ UTC-PD.

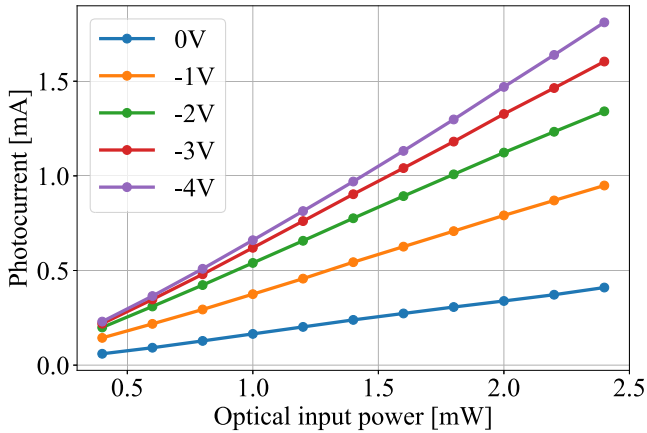


Fig. 5. Measured photocurrent as function of optical input power for PD of size $5 \times 2 \mu\text{m}^2$, showing clear bias dependence.

be circumvented by adding band smoothing layers in between the interface.

The measured external responsivities are shown in Fig. 6 for UTC-PDs with different configurations at -4 V bias and 2 mW input power. For PDs with equal width, the responsivity increases with longer PD lengths, which is consistent with the theoretical model. There is a large fluctuation in the measured values even for PDs with same size, due to the non-uniformity in fabrication. After bonding, the thickness of the BCB layer is unevenly distributed over the chip, which causes a variation in the coupling strength of grating couplers at different positions of the chip, since the thickness of BCB layer determines the constructive or destructive diffraction of reflected light at the surface of grating couplers and at the surface of BCB/Si interface. It is worth mentioning that the green measurement points are from devices in the center region of the chip, which enjoys better stability and uniformity during the fabrication.

Using an on-chip reference waveguide array, coupling losses of the grating couplers and waveguides are calibrated out in order to determine the internal responsivity of the devices. It should however be noted that only a single reference waveguide array

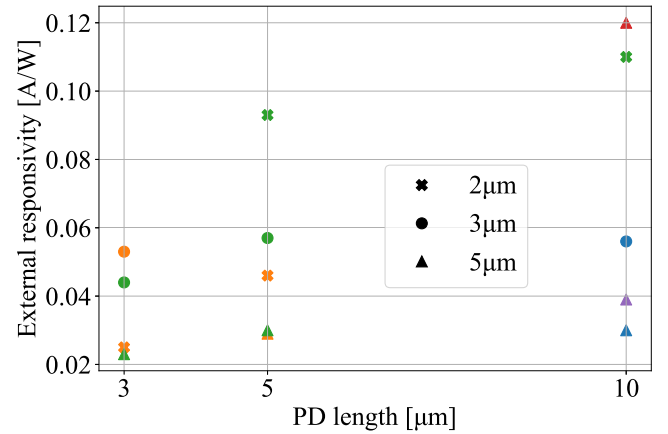


Fig. 6. External responsivity as function of device length at -4 V and 2 mW of optical input power. Colors indicate PDs at same location on wafer.

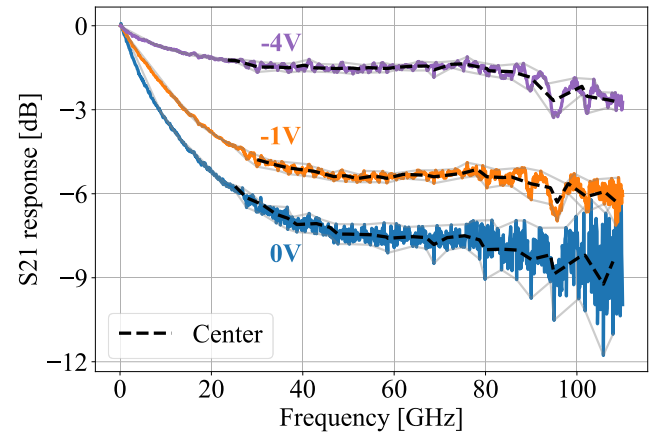


Fig. 7. S_{21} of a $5 \times 2 \mu\text{m}^2$ UTC-PD at low optical power and different bias voltages, including setup oscillation filtering, with a 3 dB bandwidth $> 110 \text{ GHz}$ at -4 V .

was available, leaving an uncertainty in the obtained internal responsivities, due to the uneven BCB layer thickness. Together with the simulated responsivity values reported in [12], the internal responsivity of the $5 \times 2 \mu\text{m}^2$ UTC-PD at -4 V bias and an input power of 2 mW is expected to be around 0.6 A/W . The $5 \times 2 \mu\text{m}^2$ PD also has a wide bandwidth as will be shown later.

B. Bandwidth Measurements

A Keysight vector network analyzer (VNA) with E/O transducer, operating in frequencies up to 110 GHz is used to determine the 3 dB bandwidth of various UTC-PDs for varying bias voltages and optical input powers, implemented as LCA in the measurement setup as depicted in Fig. 3. De-embedding on the LCA is applied to exclude influence of the electrical setup components from the device under test (DUT).

The bandwidths have been determined based on the center level of the frequency response to filter out oscillations from the measurement setup, as shown in Fig. 7 for a PD of size

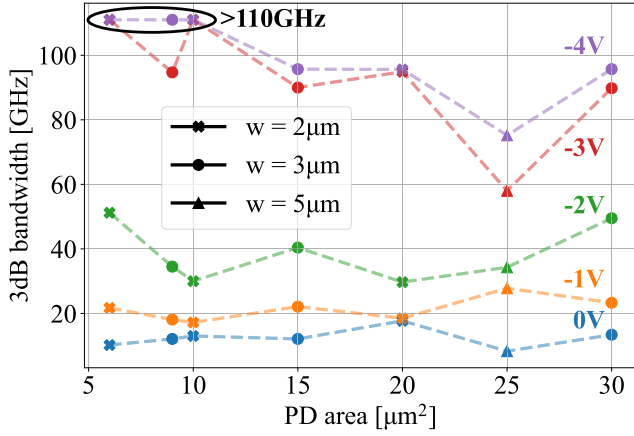


Fig. 8. 3 dB bandwidth versus PD area showing bias dependence, reaching > 110 GHz for small area PDs, measured at low optical input powers.

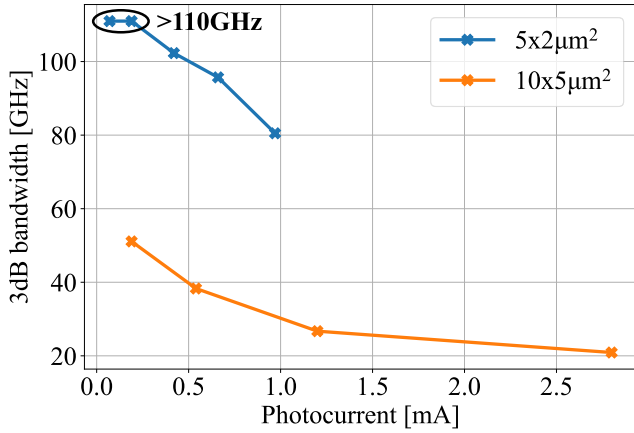


Fig. 9. 3 dB bandwidth as function of optical input power for multiple variations, showing reduced bandwidths at increased photocurrents.

$5 \times 2 \mu\text{m}^2$ at various bias voltages. The measured 3 dB bandwidth as function of the UTC-PD area is shown in Fig. 8, for increasing bias voltage. Bandwidths beyond 110 GHz are achieved for the three smallest PDs, where the bandwidth is limited by the transit time. Using the electrical equivalent model introduced in the next section, f_{RC} is determined to be 203.8 GHz for a PD of size $5 \times 3 \mu\text{m}^2$. With (1) and a $f_{3\text{dB}}$ of 95.7 GHz, f_{tr} is calculated to be 108.4 GHz which corresponds to value expected from theory. The figure shows a high bias dependence on the 3 dB bandwidth, with an optimal point around -4 V. This dependence is caused by the lack of band-smoothing layers causing a discontinuity in the band structure between the p-InGaAs absorption layer and the i-InP collection layer [12]. Bandwidth reduction at larger PD area follows from the increased RC constant of the larger area photodiodes, validating the design choice to fabricate smaller area PDs in order to boost the bandwidth. The increased series resistance of the $5 \mu\text{m}$ wide PDs significantly reduces the bandwidth as shown in the figure at a PD area of $25 \mu\text{m}^2$.

The 3 dB bandwidth is also determined as a function of the photocurrent. This is achieved for two different variations as indicated in Fig. 9. The figure shows that the 3 dB bandwidth

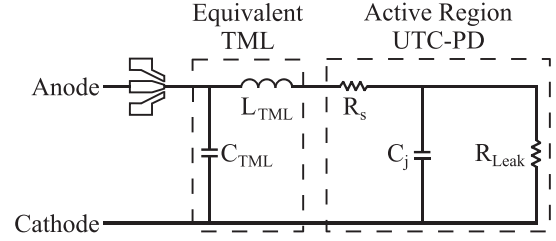


Fig. 10. Electrical equivalent circuit of the UTC-PD.

reduces for increasing photocurrents, for both variations at all bias voltages, likely caused by multiple factors. Due to the lack of band-smoothing layers, the carriers can get trapped at the InGaAs/InP interface, increasing their transit time [12]. Moreover, the increased optical power raises the temperature inside the PD, limiting the transit speed of the electrons in both the absorption and collection layer [22], increasing the transit time and reducing the overall bandwidth.

Since the optimal 3 dB bandwidth corresponds to low optical input powers, whereas the optimal responsivity corresponds to high optical input powers, the bandwidth efficiency product is a result of the trade-off. The highest achieved bandwidth efficiency product at 50.7 GHz corresponds to a PD of size $5 \times 2 \mu\text{m}^2$ at low optical input powers.

C. Electrical Equivalent Circuit

To determine the effects on series resistance and junction capacitance by reducing the area of the UTC-PD, an electrical equivalent circuit was synthesized based on S22 measurements [23], using an Agilent vector network analyzer up to 67 GHz as LCA in the setup depicted in Fig. 3. S22 measurements are conducted for all size variations under the dark regime where no light is applied at the input of the device. Measurements at different photocurrents are conducted for a limited number of variations.

As depicted in Fig. 10, the equivalent circuit is split in three elements, being the UTC-PD itself, a transmission line section and the GSG pads. The transmission line section of the circuit is based on open and short circuit on-wafer measurements and is modelled by a capacitance of 18 fF and an inductance of 64 pH for all variations. The parameter values of all components are obtained by fitting the frequency response of the equivalent model to the S22 measurements. The leakage resistance R_{Leak} between the anode and cathode corresponds to a leakage current from the PD to the substrate which is responsible for the drop in the S21 response in the first 30 GHz in Fig. 7.

The extracted R_s and C_j as function of device area are calculated in Figs. 11 and 12 respectively. As shown in Fig. 11, R_s increases for wider devices, which is due to the increased separation of the p-contacts beneath the absorption area of the UTC as explained. Next to this, the figure shows a decrease in R_s for increasing device length. This is due to the increase of junction area for longer PDs. It should be noted that the series resistance in particular for smaller devices is difficult to extract with high accuracy, due to the very large total impedance [12].

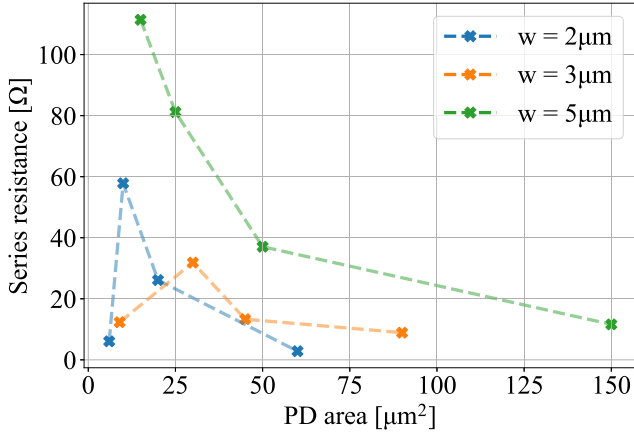


Fig. 11. R_s as function of PD area for specified widths and bias voltages.

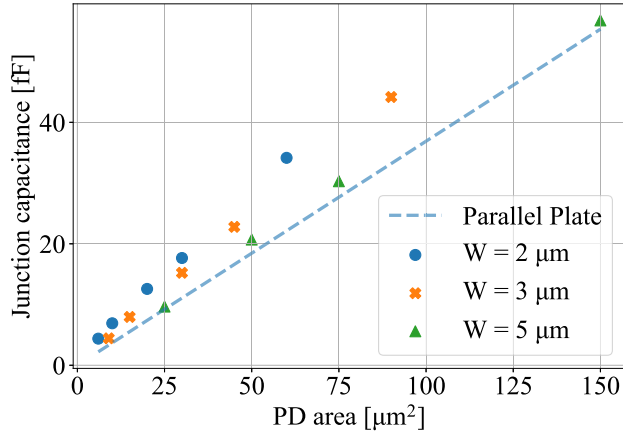


Fig. 12. C_j as function of PD area, compared to theoretical value from parallel plate model at zero bias.

The junction capacitance as function of device area in Fig. 12 is compared to the theoretical value based on the parallel plate model which it follows with minimal error, in particular for devices with a width of 5 μm . The difference in slope for the 2 & 3 μm wide devices may be caused by a parasitic capacitance due to leakage of the electric field around the edges of the structure. This results in a fringe capacitance parallel to the junction capacitance [24], [25]. The figure indicates that C_j as low as 4.4 fF is achieved, which combined with the series resistance of the same device of 6.5 Ω , results in a high f_{RC} . This confirms the effect of the design choice of PD area reduction resulting in high bandwidths.

D. C_j as Function of Photocurrent and Bias Voltage

The junction capacitance is also determined as a function of photocurrent. The analysis of PDs of sizes $10 \times 2 \mu\text{m}^2$ and $3 \times 5 \mu\text{m}^2$ are shown in particular in Fig. 13. For both sizes, an increased reverse bias voltage reduces the junction capacitance, caused by the increased electric field inside the PD that widens the depletion region and decreases the carrier build up in the PD. Additionally, the junction capacitance increases for higher

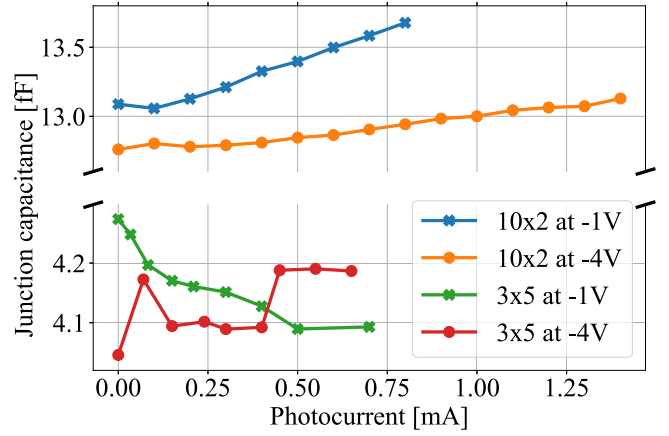


Fig. 13. C_j as function of photocurrent for two sizes and two bias voltages, showing positive and negative differential capacitance. Note y-axis break and scale difference.

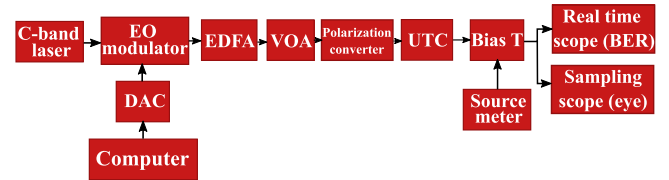


Fig. 14. Schematic representation of the data transmission measurement setup.

photocurrents for size $10 \times 2 \mu\text{m}^2$ which follows from accumulation of carriers due to the increased optical power [26]. However, size $3 \times 5 \mu\text{m}^2$ shows a decrease in junction capacitance for a low photocurrent. This follows from the voltage drop over the higher series resistance due to increased photocurrents [27]. The bias voltage across the junction is reduced due to this, which could cause variations in the junction capacitance [28]. The negative differential capacitance (NDC) for the 5 μm wide PDs follows from the higher series resistance for this width, as can be observed in Fig. 11. The effect is less pronounced at increased reverse bias due to the smaller relative voltage drop. Also, at increased photocurrents, other effects such as charge accumulation start to become more prominent and influence the junction capacitance.

E. Data Transmission Measurements

Data transmission measurements are performed to demonstrate the performance of the UTC-PD in optical interconnects and telecommunications. The measurement setup schematically depicted in Fig. 14 was used for this measurement where an optical laser at 1550 nm was amplitude modulated using an electro-optical modulator controlled by a digital to analog converter (DAC) operating at 120 GSa/s. The modulated signal was amplified using an EDFA and a variable optical attenuator (VOA) was used to carefully set the optical input power into the UTC-PD. The electrical output of the UTC-PD was connected to a sampling scope for eye diagram measurements and a 160 GSa/s real-time scope for BER measurements.

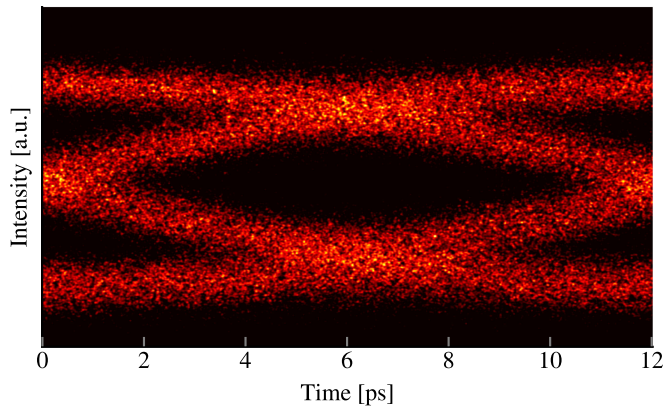


Fig. 15. Open OOK eye diagram before equalization for PD of size $10 \times 3 \mu\text{m}^2$ at 75 GBaud and raised-cosine pulse shaping with roll-off of 0.33.

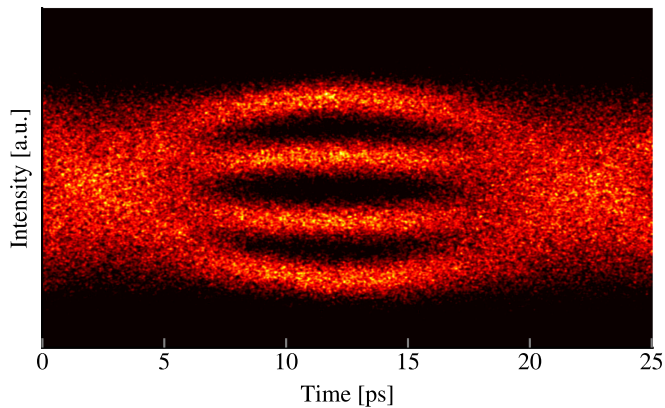


Fig. 16. Open PAM4 eye diagram before equalization for PD of size $10 \times 3 \mu\text{m}^2$ at 50 GBaud and without pulse shaping.

For BER measurements, both On-Off Keying (OOK) and four level Pulse Amplitude Modulation (PAM4) pulse shaped sequences containing 2^{16} pseudo-random symbols at increasing baud-rates were used. The captured sequences were resampled to 2 samples-per-symbol and equalized by a 51 tap decision-directed least-mean-square equalizer, after which bit errors are counted over 16 million samples. No errors were observed during the transmission of OOK modulation up to 75 GBaud, corresponding to the eye diagram in Fig. 15, for a PD of size $10 \times 3 \mu\text{m}^2$. Using PAM4 modulation, BER values lower than the 6.7% overhead hard-decision forward error correction (HD-FEC) at 3.84×10^{-3} [29], are measured for symbol rates of up to 62.5 GBaud as shown in Fig. 17, resulting in a net data rate of 117 Gb/s. An open eye diagram using PAM4 modulation at 50 Gbaud is shown in Fig. 16.

The measured 3 dB bandwidths suggest transmission rates beyond 100 GBaud, which was however not achieved due to the bandwidth reduction at the relatively high photocurrent operation point, necessary to achieve sufficient voltage swing into the electrical scope. Additionally, the inefficient on-chip grating couplers with an average insertion loss of 11 dB drastically reduce the total responsivity of the device. The obtained

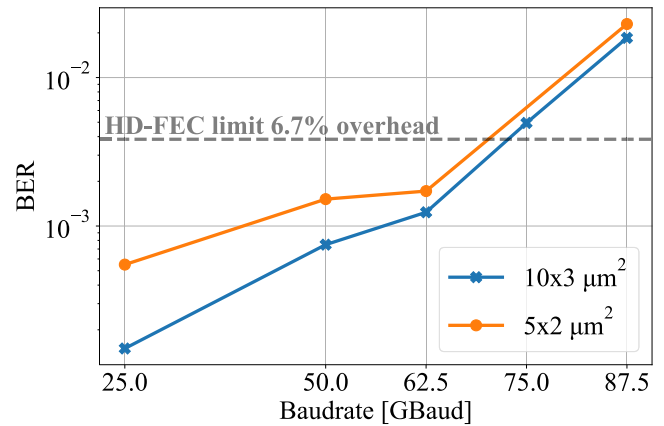


Fig. 17. Bit error rate as function of baudrate for PAM4 for two PDs and raised-cosine pulse shaping with roll-off of 0.01.

results demonstrate that the UTC-PD can be used for high capacity applications in telecommunications. The mismatch in optimal photocurrent operation point between the bandwidth and responsivity is limiting the data transmission measurements due to an inferior signal to noise ratio at low photocurrent (high bandwidth) and reduced bandwidth at high photocurrent (high responsivity).

IV. CONCLUSION

An improved UTC-PD design at reduced footprints based on [12] and its detailed characterization are presented in this work. The waveguide integrated uni-traveling carrier photodiode is realized in the InP-membrane-on-silicon platform [15]. The usage of high accuracy e-beam lithography results in high bandwidth PDs as small as $3 \times 2 \mu\text{m}^2$. Measurements demonstrate 3 dB bandwidth beyond 110 GHz, together with a maximum responsivity of 0.75 A/W for a device of $5 \times 2 \mu\text{m}^2$ in size. Both bandwidth and responsivity are photocurrent dependent, and showed opposite trends in the dependency, resulting in a trade-off in the bandwidth efficiency product.

S-parameter measurements for all size variations were used to extract equivalent circuit parameters in order to demonstrate the reduction of series resistance and junction capacitance of PDs at reduced area. By measuring the S-parameters at different points of operation, bias and photocurrent dependent junction capacitances are also included to investigate the photocurrent dependent responsivity and bandwidth. The bandwidth reduction at increased photocurrents is explained by various factors such as charge accumulation, carrier trapping and reduced carrier velocity due to heat generation.

Data transmission measurements were used to demonstrate the high speed telecommunications capabilities of the UTC-PD. Pre-FEC BERs below the 6.7% overhead HD-FEC threshold were observed for PAM4 signals with a net data rate of 116 Gb/s, and no errors were observed during OOK signal transmission up to 75 GBaud.

Based on the observed bias dependence and bandwidth reduction at increased photocurrents, both mainly caused by the band discontinuity at the InGaAs/InP interface, the addition of band-smoothing layers can be implemented in the next-generation design. The expected bias voltage reduction also decreases the heat generation during operation, increasing the free carrier drift velocity.

The improved design at smaller footprints results in a high bandwidth and high efficiency waveguide integrated UTC-PD, which can directly be integrated with passive optical devices in the InP-membrane-on-silicon platform. The results demonstrate a promising device for high speed telecommunications and emerging imaging techniques using frequencies up to the terahertz range.

ACKNOWLEDGMENT

The authors acknowledge NanoLab@TU/e for the use of the cleanroom facilities and Chris Coleman and Ryan P. Scott at Keysight Technologies USA for the use of their 110 GHz high speed measurement equipment.

REFERENCES

- [1] M. Xiao *et al.*, "Millimeter wave communications for future mobile networks," *IEEE J. Sel. Areas Commun.*, vol. 35, no. 9, pp. 1909–1935, Sep. 2017.
- [2] T. Nagatsuma, "Terahertz applications inspired by photonics," in *Proc. Int. Conf. Infrared, Millimeter, Terahertz Waves, IRMMW-THz*, 2018, pp. 1–3.
- [3] S. Carpenter, M. Abbasi, and H. Zirath, "Fully integrated d-band direct carrier quadrature (IQ) modulator and demodulator circuits in InP DHBT technology," *IEEE Trans. Microw. Theory Tech.*, vol. 63, no. 5, pp. 1666–1675, May 2015.
- [4] I. Degli-Eredi *et al.*, "Millimeter-wave generation using hybrid silicon photonics," *J. Opt. (United Kingdom)*, vol. 23, no. 4, p. 43001, Mar. 2021.
- [5] H. Mohammadhosseini and M. J. Heck, "Silicon photonics to improve the energy-efficiency of millimeter wave communication systems," in *Proc. Int. Top. Meeting Microw. Photon.*, 2017, pp. 1–4.
- [6] S. Lischke *et al.*, "Ge photodiode with -3 dB OE bandwidth of 110 GHz for PIC and ePIC platforms," in *Proc. IEEE Int. Electron Devices Meeting*, 2020, pp. 7.3.1–7.3.4.
- [7] T. Ishibashi and H. Ito, "Uni-traveling-carrier photodiodes," *J. Appl. Phys.*, vol. 127, no. 3, 2020.
- [8] A. Beling and J. C. Campbell, "InP-based high-speed photodetectors," *J. Lightw. Technol.*, vol. 27, no. 3, pp. 343–355, Feb. 2009.
- [9] C. C. Renaud, D. Moodie, M. Robertson, and A. J. Seeds, "High output power at 110 GHz with a waveguide uni-travelling carrier photodiode," in *Proc. IEEE Lasers Electro-Optics Soc. Annu. Meeting Conf. Proc.*, 2007, pp. 782–783.
- [10] N. Shimizu, Y. Miyamoto, and T. Ishibashi, "Uni-traveling-carrier photodiodes," in *Proc. IEEELEOS Annu. Meeting Conf. Proc. 12th Annu. Meeting. IEEE Lasers Electro-Optics Soc. Annu. Meeting*, 1999, pp. 808–809.
- [11] S. Nellen *et al.*, "Experimental comparison of UTC- and PIN-photodiodes for continuous-wave terahertz generation," *J. Infrared, Millimeter, THz Waves*, vol. 41, no. 4, pp. 343–354, Apr. 2020.
- [12] L. Shen *et al.*, "High-bandwidth uni-traveling carrier waveguide photodetector on an InP-membrane-on-silicon platform," *Opt. Exp.*, vol. 24, no. 8, pp. 8290–8301, 2016.
- [13] S. Reniers, L. Shen, J. V. Engelen, K. Williams, and J. V. D. Tol, "A waveguide-coupled uni-traveling-carrier photodiode with a high bandwidth-efficiency product on an indium phosphide membrane," *Presented CSW 2021*, vol. 34, no. 9, pp. 450–451, 2020.
- [14] Y. Wang *et al.*, "InP-Based grating antennas for high-resolution optical beam steering," *IEEE J. Sel. Topics. Quantum Electron.*, vol. 27, no. 1, pp. 1–7, Jan.-Feb. 2021, Art. no. 6100107.
- [15] Y. Jiao *et al.*, "Indium phosphide membrane nanophotonic integrated circuits on silicon," *Phys. Status Solidi Appl. Mater. Sci.*, vol. 217, no. 3, 2020, Art. no. 1900606.
- [16] W. Yao *et al.*, "Towards the integration of InP photonics with silicon electronics: Design and technology challenges," *J. Lightw. Technol.*, vol. 39, no. 4, pp. 999–1009, 2021.
- [17] Z. Cao, L. Shen, Y. Jiao, X. Zhao, and T. Koonen, "200 Gbps OOK transmission over an indoor optical wireless link enabled by an integrated cascaded aperture optical receiver," in *Proc. Opt. Fiber Commun. Conf. Exhib.*, 2017, pp. 1–3.
- [18] Z. Cao *et al.*, "Ultrahigh throughput indoor infrared wireless communication system enabled by a cascaded aperture optical receiver fabricated on InP membrane," *J. Lightw. Technol.*, vol. 36, no. 1, pp. 57–67, 2018.
- [19] S. Keyvaninia, M. Muneeb, S. Stanković, P. J. V. Veldhoven, D. V. Thourhout, and G. Roelkens, "Ultra-thin DVS-BCB adhesive bonding of III-V wafers, dies and multiple dies to a patterned silicon-on-insulator substrate," *Opt. Mater. Exp.*, vol. 3, no. 1, pp. 35–46, Jan. 2013.
- [20] T. H. Stievater and K. J. Williams, "Thermally induced nonlinearities in high-speed p-i-n photodetectors," *IEEE Photon. Technol. Lett.*, vol. 16, no. 1, pp. 239–241, Jan. 2004.
- [21] M. S. Islam, A. Nespola, M. Yeahia, M. C. Wu, D. L. Sivco, and A. Y. Cho, "Correlation between the failure mechanism and dark currents of high power photodetectors," in *Proc. IEEE Annu. Meeting Conf. Proc. 13th Annu. Meeting. IEEE Lasers Electro-Optics Soc. Annu. Meeting*, 2000, pp. 82–83.
- [22] T. J. Maloney and J. Frey, "Transient and steady-state electron transport properties of GaAs and InP," *J. Appl. Phys.*, vol. 48, no. 2, pp. 781–787, 1977.
- [23] D. Konstantinou, C. Caillaud, S. Rommel, U. Johannsen, and I. T. Monroy, "Investigation of de-embedding techniques applied on uni-traveling carrier photodiodes," in *Proc. 50th Eur. Microwave Conf. (EuMC)*, pp. 320–323, 2021, doi: 10.23919/EuMC48046.2021.9338063.
- [24] M. Piels and J. E. Bowers, "40 Ghz si/ge uni-traveling carrier waveguide photodiode," *J. Lightw. Technol.*, vol. 32, no. 20, pp. 3502–3508, Oct. 2014.
- [25] W. C. Chuang, C. W. Wang, W. C. Chu, P. Z. Chang, and Y. C. Hu, "The fringe capacitance formula of microstructures," *J. Micromechanics Microengineering*, vol. 22, no. 2, 2012, Art. no. 025015.
- [26] X. Ma, Y. Huang, Y. Yang, T. Liu, X. Duan, and X. Ren, "Optical power dependence of capacitance in uni-traveling-carrier photodetectors," in *Proc. Asia Commun. Photon. Conf. ACP*, 2018, pp. 1–3.
- [27] M. Dentan and B. De Cremoux, "Numerical simulation of the nonlinear response of a p-i-n photodiode under high illumination," *J. Lightw. Technol.*, vol. 8, no. 8, pp. 1137–1144, 1990.
- [28] A. Beling, H. Pan, H. Chen, and J. C. Campbell, "Linearity of modified uni-traveling carrier photodiodes," *J. Lightw. Technol.*, vol. 26, no. 15, pp. 2373–2378, 2008.
- [29] E. Agrell and M. Secondini, "Information-theoretic tools for optical communications engineers," in *Proc. IEEE Photonics Conf.*, 2018, pp. 1–5.

Jasper de Graaf was born in Julianadorp, The Netherlands. He received the B.Sc. and M.Sc. degrees in electrical engineering from the Eindhoven University of Technology, in 2018 and 2020, respectively. During his graduation project, he worked on an integrated optical alignment sensor in collaboration with ASML. In 2020, he started the Ph.D. degree with the Photonic Integration Group within the same university. His current research interests include the novel III-V based nanophotonic platform IMOS, in particular in high speed UTC-PDs for the purpose of terahertz generation.

Xinran Zhao was born in China, in 1989. She received the B.S. degree in information engineering from the Beijing Institute of Technology, Beijing, China, in 2011, and the M.S. degree in electrical engineering from the Eindhoven University of Technology, Eindhoven, the Netherlands, in 2015. In 2015, she started working toward the Ph.D. degree with the Electro-Optical Communications Group Eindhoven University of Technology, engaging in research on the design and fabrication of integrated receivers for free space optical communication systems.

Dimitrios Konstantinou received the Diploma in electrical and computer engineering from the National Technical University of Athens, in 2015, the master's studies in telecommunications with a specialty from the Technical University of Denmark, in 2017. Since October 2017, he is a Doctorate Candidate with the Eindhoven University of Technology (TU/e). He is part of the ITN European Project 5G STEP FWD with focus on the synthesis of High Speed 5G Base Stations combining Photonic and Electronic Integration on InP.

Menno van den Hout (Student Member, IEEE) was born in Veghel, The Netherlands, in 1995. He received the B.Sc. and M.Sc. (*cum laude*) degrees in electrical engineering from the Eindhoven University of Technology, The Netherlands, in 2017 and 2019, respectively, on the topic of transmitter optimization in coherent optical transmission systems. He is currently working toward the Ph.D. degree on the subject of wideband spectral/spatial agile optical transmission systems with the High Capacity Optical Transmission Laboratory, Electro-Optical Communications group, at Eindhoven University of Technology.

Sander Reniers was born in Hapert, The Netherlands. He received the B.Sc. and M.Sc. degrees in electrical engineering from the Eindhoven University of Technology, in 2014 and 2017, respectively. He is currently working toward the Ph.D. degree with the same university. His research interests include waveguide reflectors and polarization diversity on the IMOS platform.

Longfei Shen was born in Beijing, China, in 1988. He received the bachelor's degree in electrical engineering from Zhejiang University, Hangzhou, China, in 2010, the master's degree in 2012, with a thesis project performed at Philips Research, and the Ph.D. degree (*cum laude*) from the Eindhoven University of Technology, Eindhoven, the Netherlands, in 2016, based on research in high-speed photodetectors and heterogeneous integration technology. He subsequently moved to Europe to study photonics with the Royal Institute of Technology (KTH), supported by the Erasmus Mundus scholarship.

Sjoerd van der Heide (Student Member, IEEE) was born in 's-Hertogenbosch, the Netherlands, in 1992. He received the B.Sc. and M.Sc. (*cum laude*) degrees in electrical engineering from the Eindhoven University of Technology, the Netherlands, in 2015 and 2017, respectively. He is currently working toward the Ph.D. degree with the High-Capacity Optical Transmission Laboratory, Electro-Optical Communications Group, at the Eindhoven University of Technology. His research interests include space-division multiplexing and digital signal processing. He was the recipient of a Student Paper Award at ECOC 2018, a Best Paper Award at OECC 2019, and a Student Paper Award at ECOC 2020.

Simon Rommel (Member, IEEE) received the B.Sc. degree from the University of Stuttgart, Germany, in 2011 and the M.Sc. degree in photonic networks engineering from Aston University, Birmingham, U.K., in 2014, and Scuola Superiore Sant'Anna, Pisa, Italy. He completed the Ph.D. degree in 2017 with the Technical University of Denmark, Kongens Lyngby, Denmark with research focused on photonic-wireless convergence and millimeter-wave radio-over-fiber links. In the same year he visited the National Institute of Information and Communications Technology, Koganei, Tokyo, Japan for a research stay. Since 2017, he is with Eindhoven University of Technology, currently as an Assistant Professor, continuing his work on photonic and radio frequency technologies with a strong focus on implementations beyond 5G. His research interests include the fields of fiber-optic and wireless communications and the associated digital signal processing. He has contributed to multiple national and European research projects, incl. H2020 blueSPACE as a Technical Manager. Dr. Rommel is a Member of Institute of Electrical and Electronics Engineers (IEEE), The Optical Society (OSA), the Institution of Engineering and Technology (IET) and the Verband der Elektrotechnik Elektronik Informationstechnik e.V (VDE).

Idelfonso Tafur Monroy graduated from the Bonch-Bruевич Institute of Communications, St. Petersburg, Russia, in 1992, where he received the M.Sc. degree in multichannel telecommunications. In 1996, he received the Technology Licentiate in telecommunications theory from the Royal Institute of Technology, Stockholm, Sweden. In same year, he joined the Electrical Engineering Department, Eindhoven University of Technology, the Netherlands, where he received the Ph.D. degree in 1999 and worked as an Assistant Professor until 2006. He founded in 2008 and led until 2017, the Metro Access and Short Range Communications Group of the Department of Photonics Engineering, Technical University of Denmark. He currently is affiliated with the Electrical Engineering Faculty with TU/e. He participated in several European research framework projects in photonic technologies and their applications to communication systems and networks. His research interests include Terahertz wireless communication and sensing systems, quantum secure digital infrastructures, and application of nanophotonic technologies in communications and security.

Chigo Okonkwo (Senior Member, IEEE) was born in Wakefield, U.K., in 1979. He received the Ph.D. degree in optical signal processing from the University of Essex, Colchester, U.K., in 2010. Between 2003 and 2009, he was a Senior Researcher with Photonic Networks Research Lab, University of Essex, U.K. After the Ph.D. degree, he was appointed as a Senior Researcher with the Electro-Optical Communications Group, working on digital signal processing techniques and the development of space-division multiplexed transmission (SDM) systems. He is currently an Associate Professor and leads the High Capacity Optical Transmission Laboratory, Institute for Photonic Integration (former COBRA), Department of Electrical Engineering, Eindhoven University of Technology, Eindhoven, The Netherlands. He was instrumental to the delivery of the first major SDM project in the European Union-MODEGAP project. Since 2014, he has been tenured with the ECO Group, where he has built up a world-class laboratory collaborating with several industrial and academic partners. His research interests include optical and digital signal processing, space-division multiplexing techniques, and long-haul transmission techniques. In 2018, he was the TPC Chair for subcommittee three on digital signal handling. Between 2015 and 2017, he was on the TPC for the OSA Conference on Signal Processing in Photonic Communications (SPPCom). In 2017 and 2018, he was the Program Chair and the Conference Chair with SPPCom. He was an Associate Editor for special edition of the IEEE JOURNAL ON LIGHTWAVE TECHNOLOGY. From 2020 to 2022, he has been retained on Technical Programme Subcommittee on Fiber-Optic and Waveguide Devices and Sensors (subcommittee D5) at Optical Fiber Communications Conference.

Zizheng Cao (Member, IEEE) received the B.Sc. degree in electronic information science and technology from Hunan Normal University, Changsha, China, and the Master of Engineering on telecom engineering (awarded “Outstanding thesis of master’s degree” of Hunan Province, 2010) from Hunan University, Changsha, China. In 2015, he received the Ph.D. degree (with highest Hons.) from the Eindhoven University of Technology (TU/e). He is the recipient of a Graduate Student Fellowship (10 recipients globally) from the IEEE Photonics Society in 2014 and the recipient of TU/e doctoral project award in 2016. Dr. Cao started his Tenure Track Assistant Professor in 2016 and received the tenured position in 2018. He is the European Conference on Optical Communication (ECOC) as a Technical Program Committee (TPC) Member. He is a Member of the IEEE Photonics Society. Dr. Cao has authored or coauthored more than 180 articles, including 26 first-author journal articles, including one article in *Nature Light Science & Applications*, one cover article in *Wiley Laser and Photonic Review*, one invited paper and one postdeadline paper in *IEEE JOURNAL OF LIGHTWAVE TECHNOLOGY*, and one invited review in *IEEE JOURNAL OF QUANTUM ELECTRONICS*. He gave a series invited talks at international conferences such as PIERS2014, WOCC2016, MWP2017, ACP (2015/2017/2019), and Photonics West 2017/2019. He also coorganized IEEE Summer Topical Meeting in 2019. Till July 2020, his research articles have been cited for 1634 times, with H-index of 21 (source: scopus).

Ton Koonen (Fellow, IEEE) received the M.Sc. (with Hons.) degree in electrical engineering from TU/e in 1979. In that year, he joined Philips Telecommunicatie Industrie (Telecommunications Industry). From 1987 to 2000, he worked on high-speed transmission systems and optical fiber systems for hybrid access networks with Bell Laboratories within Lucent. He has also worked as a Professor with the University of Twente, holding a Chair on Photonic Networks. Ton is the Chairman of the Electro-Optical Communication Systems (ECO) group, part of the COBRA institute and from September 2012, he was also the Vice-Dean of the Department Electrical Engineering. Ton is a Bell Labs Fellow, OSA Fellow, ERC Advanced Investigator Grant Winner, Distinguished Guest Professor of Hunan University, Changsha, China, and has frequently acted as an auditor and reviewer on national and EC projects. He is currently involved in a number of access/in-home projects in the Freeband program, the IOP GenCom program, and the EC FP6 IST and FP7 ICT programs. He has authored and coauthored more than 250 conference and journal publications.

Kevin Williams (Member, IEEE) received the B.Eng. degree from The University of Sheffield, Sheffield, U.K., and the Ph.D. degree from the University of Bath, Bath, U.K., in 1995. He moved to the University of Cambridge, Cambridge, U.K., in 2001, where he was elected as a Fellow with the Churchill College. He is currently the Chair of the Photonic Integration Research Group, Eindhoven University of Technology, The Netherlands. His research interest includes integrated photonic circuits. He was the Recipient of the Royal Society University Research Fellowship from the University of Bristol, Bristol, U.K., in 1996. In 2006, he was the recipient of the European Commission Marie Curie Chair from the Institute for Photonic Integration (formerly COBRA Institute), Eindhoven University of Technology. In 2011, he was the recipient of the Vici Award from the Netherlands Organization for Scientific Research, where he has focused on photonic integration technology.

Yuqing Jiao (Senior Member, IEEE) was born in Hangzhou, China. He received the Ph.D. degrees from the Eindhoven University of Technology, The Netherlands, and Zhejiang University, China, in 2013. Since then, he has continued his research with the Eindhoven University of Technology. Since 2016, he has been appointed as an Assistant Professor with the Institute of Photonic Integration (IPI, former COBRA Research Institute), Eindhoven University of Technology. He has been tenured since 2018. He has (co)authored more than 50 international journal publications, among which five are invited. His research topic is focused on a novel III-V-based nanophotonic platform, where ultrafast and strong light-matter interactions occur in sub-micrometer optical confinement. The applications span from optical interconnects and terahertz photonics, to optical sensing and metrology. He has a strong background in a range of photonic materials (from silicon to III-V) and nanotechnologies. He is a Senior Member of the IEEE Photonics Society. He currently is the Board Member of the IEEE Photonics Society Benelux Chapter, and the Editorial Board Member of the *IOP Journal of Semiconductors*. He was TPC Member of several conferences: OFC 2020–2022, OECC/PSC 2019, and ACP 2020–2021.